Supporting Information

Highly anisotropic thermal conductivity of layer-by-layer assembled nanofibrillated cellulose/graphene nanosheets hybrid films for thermal management

Na Song,[*‡] Dejin Jiao,[‡] Siqi Cui, Xingshuang Hou, Peng Ding[*] and Liyi Shi

Research Center of Nanoscience and Nanotechnology, Shanghai University, 99 Shangda Road, Shanghai 200444, China

[*] Corresponding authors: FAX: +86 21 66134726. E-mail address: snlxf@shu.edu.cn (Na Song), dingpeng@shu.edu.cn (Peng Ding)

[‡] These authors contributed equally.

1. Experimental section

Preparation of Graphene Oxide. GO was synthesized from natural graphite powder using a modified Hummer's method.[1] Briefly, graphite powder (4 g), concentrated H_2SO_4 (92 mL) were stirred together in an ice bath, and $KMnO_4$ (12 g) was added quite slowly. Subsequently, the mixture was heated to 35 °C and continuously stirred for 2 h. Then, the mixture was diluted with deionized (DI) water (184 mL) and stirred for 15 min. Afterwards, additional DI water (280 mL) was added, followed by the drop-wise addition of H_2O_2 (10 mL). The suspension was vacuum-filtered and washed with HCl solution (1:10), and it was successively washed with DI water for more than 15 times until a pH of 7 was obtained. The filter cake was re-dispersed in water and sonicated for 1 h. After centrifugation at 5000 rpm for 5 min, a yellowish-brown GO dispersion was obtained.

Preparation of Nanofibrillated Cellulose. The NFC was prepared according to the method reported by Saito.[2] Cellulose fibers (cellulose content of 2 g) were suspended in DI water (200 mL) that contained TEMPO (0.025 g) and NaBr (0.25 g). The oxidation reaction of the cellulose slurry was initiated by adding the desired amount of the NaClO solution (10 mmol•g^{-1} cellulose), and the reaction continued at room temperature with stirring for 6 h. The pH of the reaction solution was maintained at 10 by adding 0.5 M of NaOH. The oxidized cellulose was thoroughly washed with DI water by filtration on a filter membrane (PTFE, 0.45 μm). Subsequently, 2 mg•mL^{-1} of the oxidized

cellulose/water slurries were sonicated for 15 min at a power of 300 W in an ice bath using an ultrasonic generator with a probe tip that had a diameter of 15 cm. Then, the slurry was centrifuged at 8000 rpm for 10 min to remove the un-nanofibrillated cellulose. The transparent NFC suspension was stored at 4 °C before use.

2. Zeta potential test

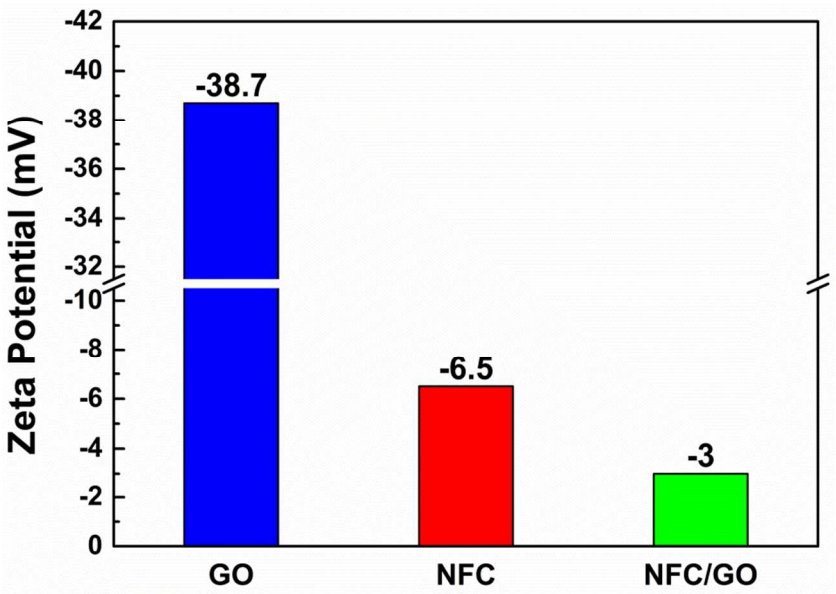

Figure S-1. Zeta potentials of GO, NFC and NFC/GO (GO content is 5 wt%) dispersions.

3. TEM image of NFC/GO hybrids

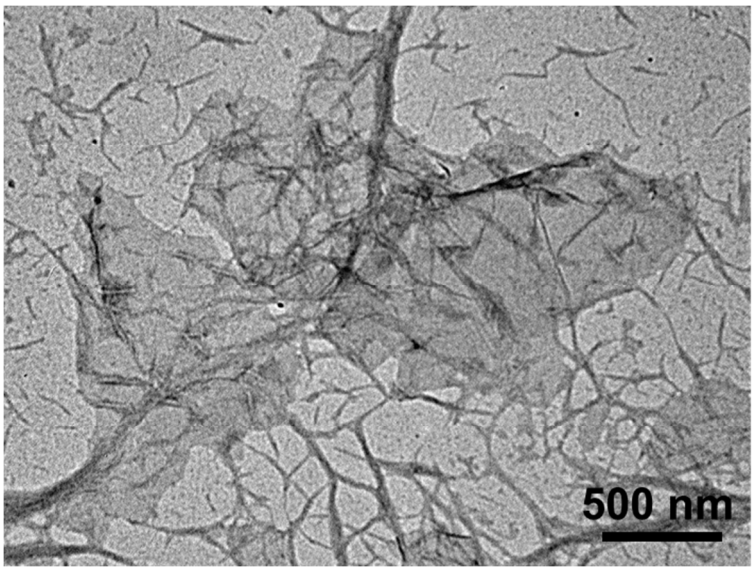

Figure S-2. TEM image of the NFC/GO hybrids in mixing dispersion (GO content is 5 wt%).

4. TGA test

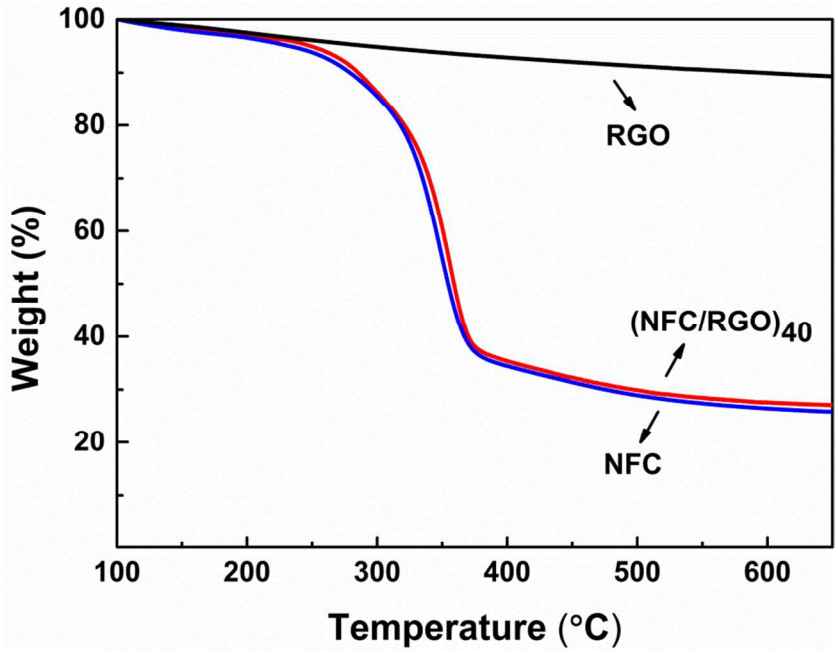

Figure S-3. TGA curves of RGO, NFC and $(NFC/RGO)_{40}$ hybrid film.

The RGO content in the $(NFC/RGO)_{40}$ hybrid film was evaluated from the TGA plot shown in Figure S2. It can be seen that the RGO nanosheets indicate the thermal stability, and only 9.0% mass loss occurs upon heating up to 650 °C. The curves of NFC and $(NFC/RGO)_{40}$ exhibit dramatic mass loss from around 200 to 400 °C due to the decomposition of cellulose chains. The mass loss from 650 °C are detected to be 73.9 and 73.0% respectively for NFC and $(NFC/RGO)_{40}$ hybrid film. The slightly increase in of residues is due to increase in amount of the RGO nanosheets. And the actual weight ratios of RGO to NFC can be inferred to be 1.0 wt% from the difference quantity of residues.[3-4]

5. SEM image of one time deposition of NFC on an ultrathin GO film

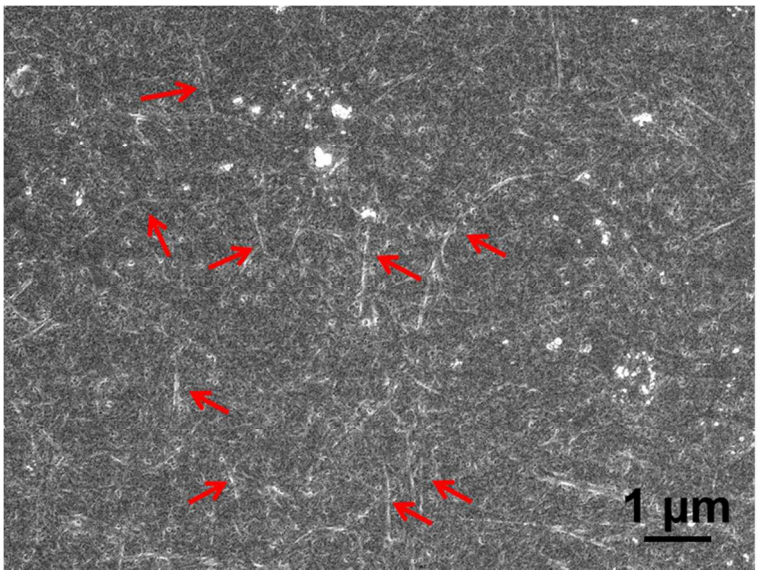

Figure S-4. Surface SEM image of the film fabricated using one time deposition of NFC on an ultrathin GO film. The red arrows demonstrate the typical NFC nanofibers exist on the top.

6. Quantitatively characterization of the degree of orientation of RGO nanosheets

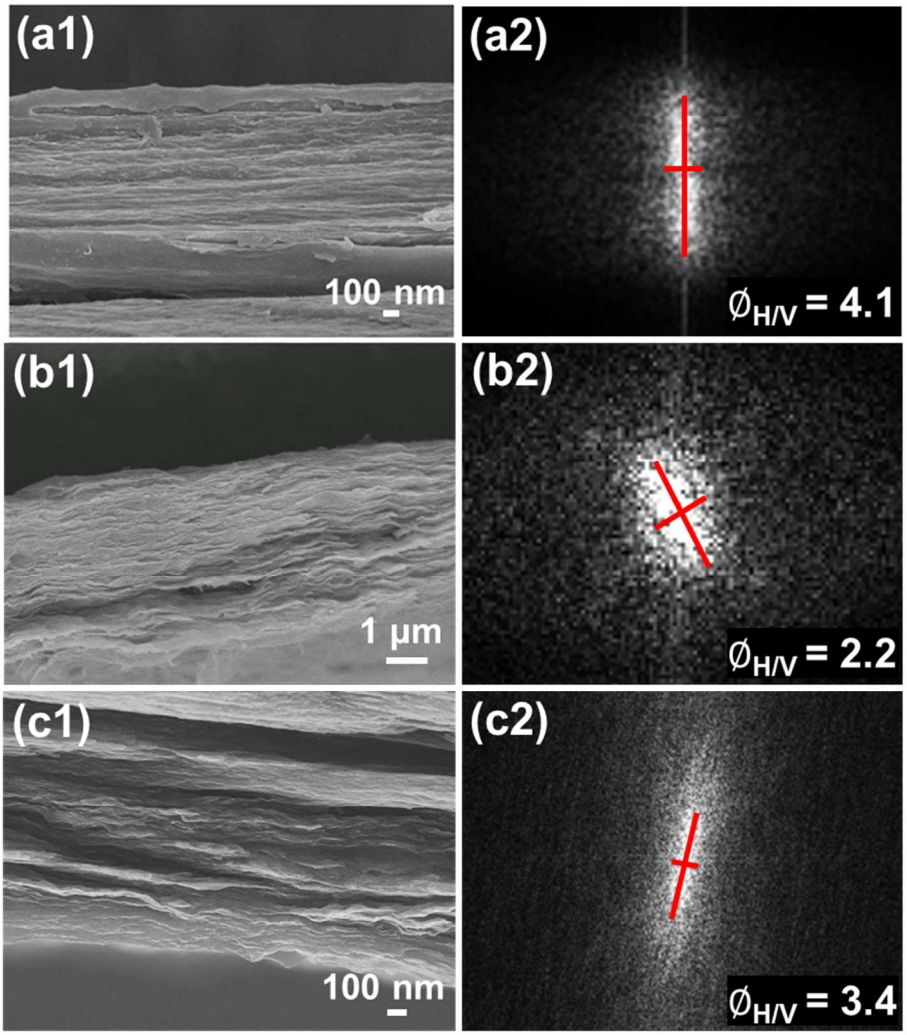

Figure S-5. (1) Cross-sectional SEM images and (2) FFT frequency domain images of (a) the thermally conductive coating prepared using LbL assembly in the present study, (b) the NFC/RGO hybrid film prepared using vacuum assisted self-assembly,[5] (c) the thermally conductive coating after 500 mechanical bending cycles.

Generally, the higher $\Phi_{H/V}$ represents the higher degree of orientation of nanosheets. It can be noted the thermally conductive coating in the $(NFC/RGO)_{40}$ hybrid film exhibits a higher $\Phi_{H/V}$ compared with the layered-structured NFC/RGO hybrid film prepared using vacuum assisted self-assembly, revealing a higher degree of orientation of RGO

nanosheets achieved by LbL assembly. And this result reveals that the LbL assembly technique is an efficient and governable method to fabricate the aligned graphene structure.

7. The thermal conductivity measurement using laser flash method

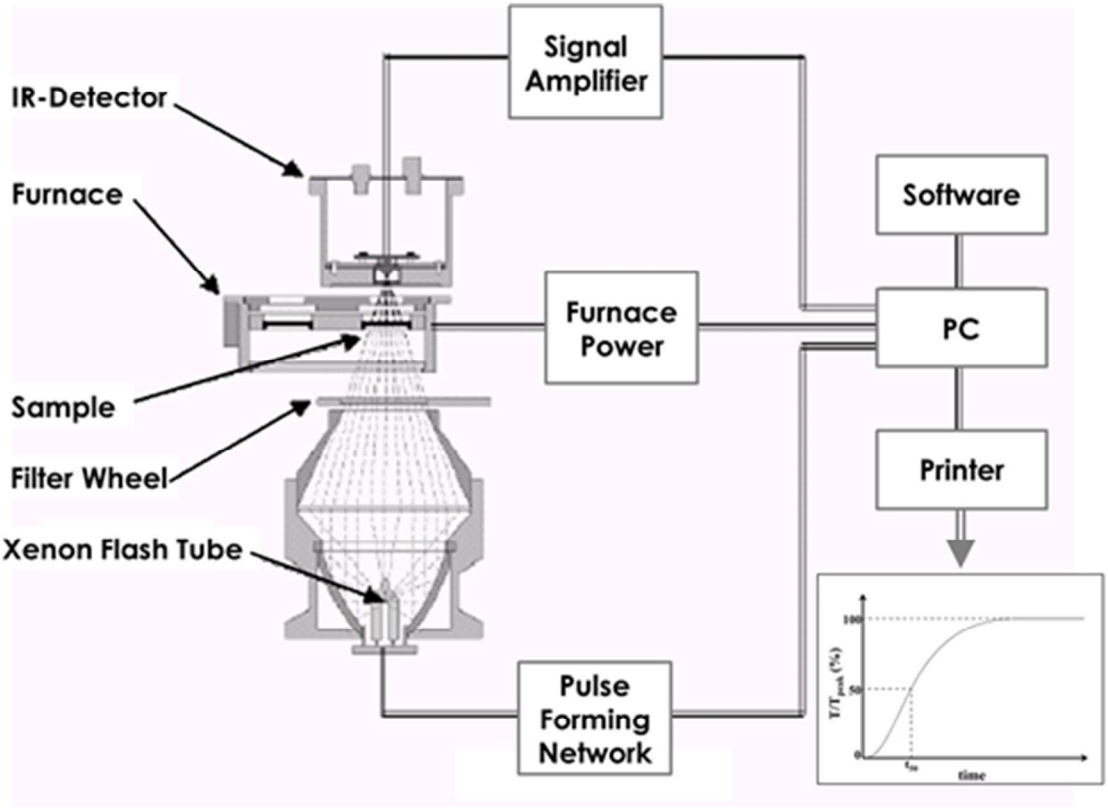

Figure S-6. Schematic diagram of thermal conductivity measurement by laser flash technique.

In this work, the thermal conductivities were measured by transient laser flash technique using Netzsch LFA 447 Nanoflash at 25 °C.[6-10] The laser flash technique is a transient method that directly measures the thermal diffusivity (α). The schematic diagram of the testing mechanism in laser flash technique was shown in Figure S-6. The laser flash technique uses a xenon flash lamp to heat the sample from the bottom side by producing shots with energy of 10 J/pulse. The temperature of the opposite surface is monitored with the nitrogen-cooled InSb IR detector. The output of the temperature

detector was amplified and adjusted for the initial ambient conditions. The recorded temperature rise curve was the change in the sample temperature resulting from the firing of the flash lamp. The magnitude of the temperature rise and the amount of the light energy were not required for a diffusivity determination; only the shape of the curve was used in the analysis. From the analysis of the resulting relative temperature (T/T peak)-time curve, the α can be extracted. The specific heat capacity (Cp) was measured with laser flash technique by comparing the magnitude of the temperature rise of the sample with that of reference calibration sample under the same experiment conditions (Cp of the reference Pyrex was approximately 0.76 $J \bullet g^{-1} \bullet K^{-1}$). The accuracy of laser flash technique measurement with Netzsch instruments is ~3%. The thermal conductivity (λ) was calculated from the equation $\lambda = \alpha \bullet Cp \bullet \rho$, where ρ is the density of the sample and can be directly obtained through a density balance.

To perform measurement, each sample was placed into a special stage and sample holder (Figure S-4) that fitted its size. The diameters of the sample for in-plane and cross-plane thermal conductivity measurement were 25.0 and 12.7 mm, respectively. The in-plane thermal conductivity measurement requires a special sample holder where the location for the light input on one side of the sample and location for measuring the temperature increase on the other side are at different lateral positions. As show in Figure S-4, the design of the sample holder ensured that heat travelled approximately 5 mm along the plane direction inside the hybrid film, which is a larger distance than its

thickness (approximately 25 μm), ensuring the in-plane values for α and λ. For the cross-plane thermal conductivity measurement, contrast to the "in-plane" test mode, heat transfer predominantly along the thickness direction of the hybrid film. In addition, the thermal conductivities of each sample needed to be measured for six folds, excluded the values with large errors the average value was the final result.

The corresponding parameters are shown in Table S-1.

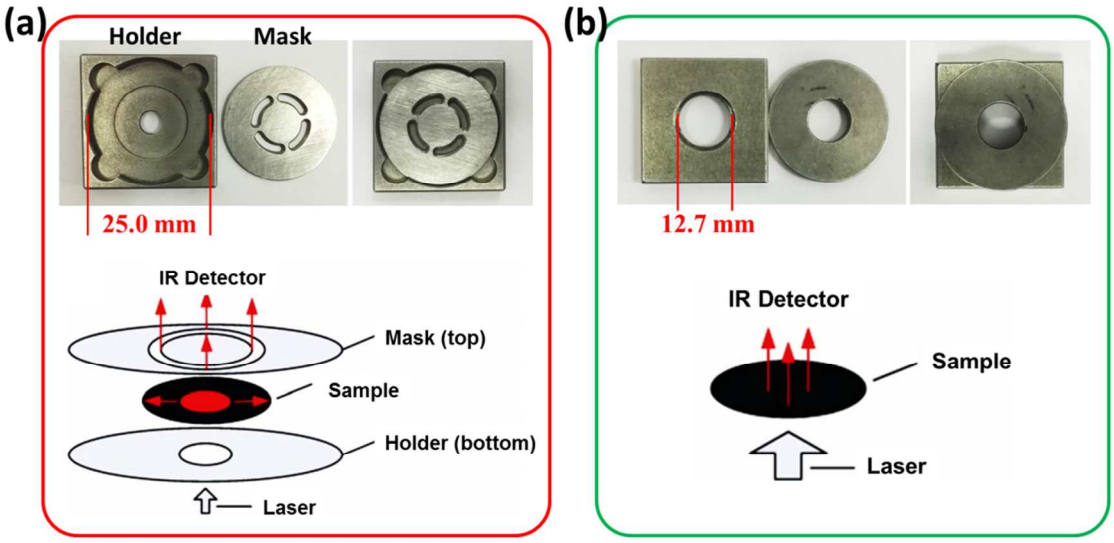

Figure S-7. The sample holders and masks used in (a) "in-plane" thermal conductivity test model; and (b) "cross-plane" thermal conductivity test model. And schematic illustrations of the directions of heat flow in two different test models using a laser flash system.[11]

Table S-1. Overview of corresponding parameters of the $(NFC/RGO)_n$ hybrid films in thermal conductivity measurement

Sample	Cp	ρ	α ($mm^2 \cdot s^{-1}$)		λ ($W \cdot m^{-1} \cdot K^{-1}$)	
$[(NFC/RGO)_n]$	($J \cdot g^{-1} \cdot K^{-1}$)	($g \cdot cm^{-3}$)	α_X	α_Z	λ_X	λ_Z
n = 0	0.728	1.270	1.212	0.037	1.121	0.034
n = 10	0.610	1.298	4.381	0.043	3.469	0.034
n = 20	0.626	1.209	8.192	0.049	6.200	0.037
n = 30	0.636	1.310	12.486	0.046	10.403	0.038
n = 40	0.607	1.255	16.376	0.059	12.475	0.045

8. Supplementary Note: Reasons for the low cross-plane thermal conductivity of NFC substrate

The NFC substrate exhibits low thermal conductivity along the cross-plane direction, and that is important for the anisotropic thermal conductivity of bulk film. Such low cross-plane thermal conductivity may be associated with the NFC's nanofibrous structure with high crystallinity and the preferential orientation of NFC in the planer direction. It is known that the main thermal transport vector in electrical insulating polymer materials and their derivatives is acoustic phonons, and the phonon transport largely depend on crystal vibrations. However, polymer materials normally have low degree of crystallinity, and the incongruous vibrations of the crystalline regions and the complex molecular chain can significantly increase the phonon scattering. These factors determine the low thermal conductivities of polymer materials.[12] Therefore, a feasible method to improve the thermal conductivity of polymers is to change their crystal structures. For example, Shen et al[13] report the fabrication of polyethylene nanofibres with the thermal conductivity as high as 104 $W \bullet m^{-1} \bullet K^{-1}$. The high thermal conductivity is attributed to the restructuring of the polymer chains by mechanical stretching, which improves degree of crystallinity and grain orientation. Alternatively, the NFC itself is a nanofiber with large aspect ratio (shown in Figure 1c). These nanofibers in turn are made of aligned crystalline elementary fibrils, which are commonly considered as the smallest morphological units in the fiber, and therefore, the NFC exhibits high degree of crystallinity (the crystallinity

index is above 55% calculate from XRD in Figure 2).[14-15] The special structure makes the NFC exhibit superior thermal conductivity along the length direction. As the NFC assembled into a frees-standing film under vacuum-filtration, the nanofibers has a tendency to form strong networks, in which the nanofibers have a good in-plane orientation, as shown in Figure 6h. And this phenomenon has also reported in prior papers.[16-17] The planer orientation of the 1D nanofibers leads to relative high in-plane thermal conductivity of the neat NFC film. On the contrary, perpendicular to the nanofibers the grain boundary within NFC, the weak interactions between NFC in radial direction, and even the porosity of bulk film can greatly increase phonon scattering. Thus, the cross-plane thermal conductivity is extremely low. Similar results have been reported in early papers. For example, Vitaliy et al[18] have reported that the cross-plane thermal conductivity of a mat composed of aligned carbon nanotube/polybenzimidazole core–shell nanofibers were only 0.010 – 0.014 $W \bullet m^{-1} \bullet K^{-1}$. The thermally insulating property was attributed to the high porosity and phonon scattering caused by the nanofibers weak interactions along the cross-plane direction.

9. Structure of the hybrid film after mechanical bending

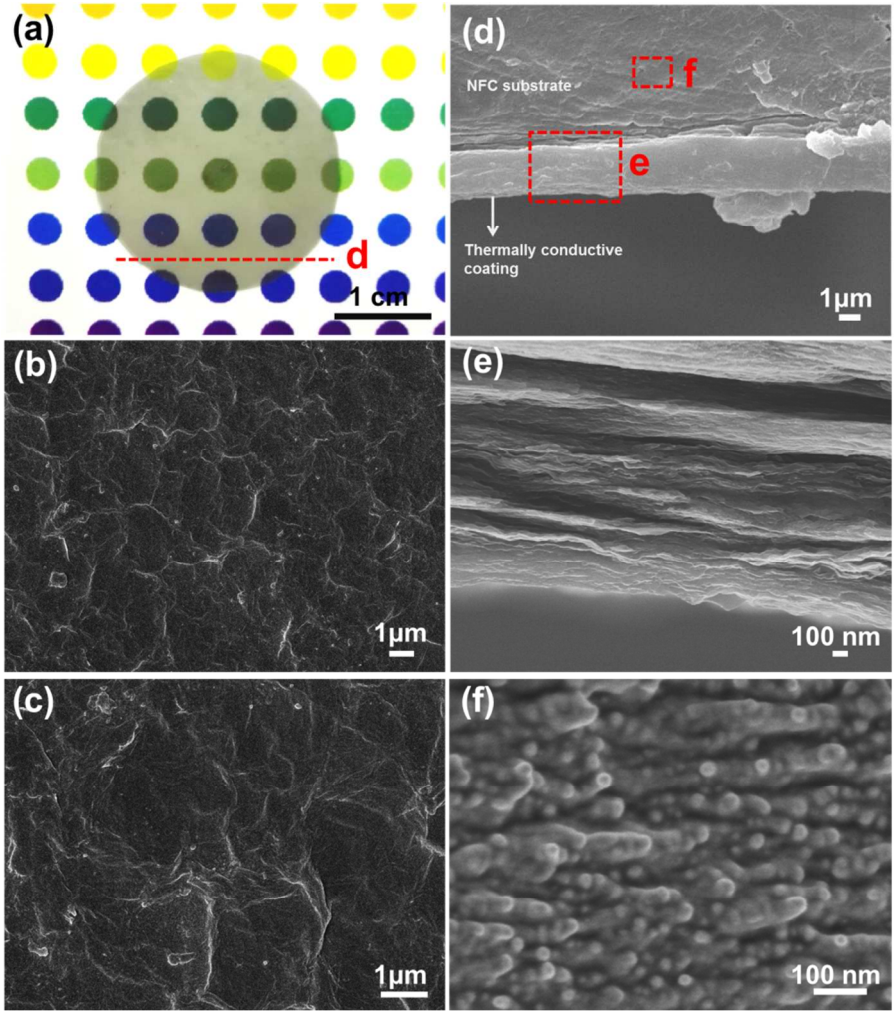

Figure S-8. (a) Photograph the $(NFC/RGO)_{40}$ hybrid film after 500 bending cycles at 135°. (b and c) The SEM images of the surface of $(NFC/RGO)_{40}$ hybrid film after 500 bending cycles. (d-f) The cross-sectional SEM images of $(NFC/RGO)_{40}$ hybrid film after 500 bending cycles, among them, (e) presents the cross-section of thermally conductive coating layer, and (f) is the NFC-substrate.

10. XPS measurement of GO and RGO

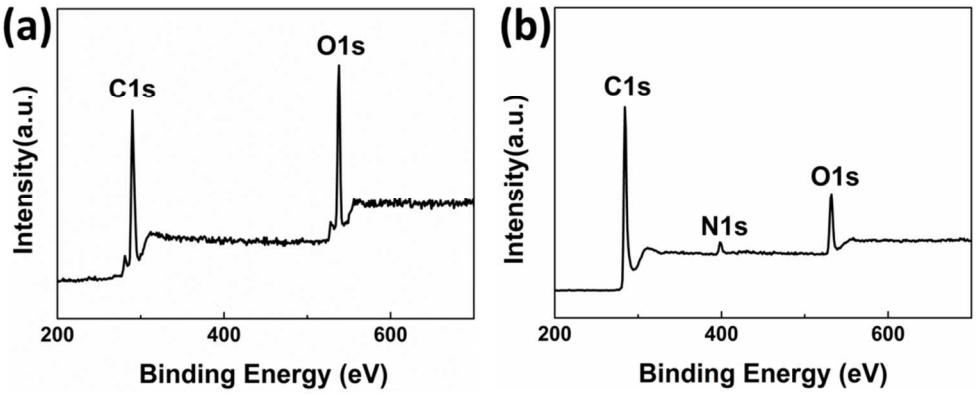

Figure S-9. The XPS spectra of (a) GO and (b) RGO.

Table S-2. The element content of N, O, C

Element content (%)	N	O	C
GO	0.62	24.88	72.51
rGO	4.09	14.10	81.81

Supplementing References

1. William S., H. J.; Richard E., O., Preparation of Graphitic Oxide. *J. Am. Chem. Soc.* **1958,** *80* (6), 1339-1339.
2. Saito, T.; Nishiyama, Y.; Putaux, J. L.; Vignon, M.; Isogai, A., Homogeneous Suspensions of Individualized Microfibrils from Tempo-Catalyzed Oxidation of Native Cellulose. *Biomacromolecules* **2006,** *7* (6), 1687-1691.
3. Wang, Y.; El-Deen, A. G.; Li, P.; Oh, B. H.; Guo, Z.; Khin, M. M.; Vikhe, Y. S.; Wang, J.; Hu, R. G.; Boom, R. M., High-Performance Capacitive Deionization Disinfection of Water with Graphene Oxide-Graft-Quaternized Chitosan Nanohybrid Electrode Coating. *Acs Nano* **2015,** *9* (10), 10142-10157.
4. Li, Q.; Guo, Y.; Li, W.; Qiu, S.; Zhu, C.; Wei, X.; Chen, M.; Liu, C.; Liao, S.; Gong, Y.; Mishra, A. K.; Liu, L., Ultrahigh Thermal Conductivity of Assembled Aligned Multilayer Graphene/Epoxy Composite. *Chem. Mater.* **2014,** *26* (15), 4459-4465.
5. Song, N.; Jiao, D.; Ding, P.; Cui, S.; Tang, S.; Shi, L., Anisotropic Thermally Conductive Flexible Films Based on Nanofibrillated Cellulose and Aligned Graphene Nanosheets. *J. Mater. Chem. C* **2016,** *4* (2), 305-314.
6. Cui, X.; Peng, D.; Nan, Z.; Shi, L.; Na, S.; Tang, S., Thermal Conductive and Mechanical Properties of Polymeric Composites Based on Solution-Exfoliated Boron Nitride and Graphene Nanosheets: A Morphology-Promoted Synergistic Effect. *ACS appl. materi. interfaces* **2015,** *7* (34), 19068-19075.
7. Ding, P.; Su, S.; Song, N.; Tang, S.; Liu, Y.; Shi, L., Highly Thermal Conductive Composites with Polyamide-6 Covalently-Grafted Graphene by an in Situ Polymerization and Thermal Reduction Process. *Carbon* **2014,** *66*, 576-584.
8. Renteria, J. D.; Ramirez, S.; Malekpour, H.; Alonso, B.; Centeno, A.; Zurutuza, A.; Cocemasov, A. I.; Nika, D. L.; Balandin, A. A., Strongly Anisotropic Thermal Conductivity of Free-Standing Reduced Graphene Oxide Films Annealed at High Temperature. *Adv. Funct. Mater.* **2015,** *25* (29), 4664-4672.
9. Jin, S.; Gao, Q.; Zeng, X.; Zhang, R.; Liu, K.; Shao, X.; Jin, M., Effects of Reduction Methods on the Structure and Thermal Conductivity of Free-Standing Reduced Graphene Oxide Films. *Diam. Relat. Mater.* **2015,** *58*, 54-61.
10. Goli, P.; Ning, H.; Li, X.; Lu, C. Y.; Novoselov, K. S.; Balandin, A. A., Thermal Properties of Graphene-Copper-Graphene Heterogeneous Films. *Nano Lett.* **2014,** *14* (3), 1497-1503.
11. Zhang, J.; Shi, G.; Jiang, C.; Ju, S.; Jiang, D., 3d Bridged Carbon Nanoring/Graphene Hybrid Paper as a High-Performance Lateral Heat Spreader. *Small* **2015,** *11* (46), 6197-6204.
12. Choy, C. L., Thermal Conductivity of Polymers. *Polymer* **1977,** *18* (10), 984-1004.
13. Shen, S.; Henry, A.; Tong, J.; Zheng, R.; Chen, G., Polyethylene Nanofibres with Very High Thermal Conductivities. *Nat. nanotechnol.* **2010,** *5* (4), 251-255.

14. Liimatainen, H.; Visanko, M.; Sirviö, J. A.; Hormi, O. E.; Niinimaki, J., Enhancement of the Nanofibrillation of Wood Cellulose through Sequential Periodate-Chlorite Oxidation. *Biomacromolecules* **2012,** *13* (5), 1592-1597.
15. Nechyporchuk, O.; Belgacem, M. N.; Bras, J., Production of Cellulose Nanofibrils: A Review of Recent Advances. *Industrial Crops and Products* **2016,** *93*, 2-25.
16. Henriksson, M.; Berglund, L. A.; Isaksson, P.; Lindström, T.; Nishino, T., Cellulose Nanopaper Structures of High Toughness. *Biomacromolecules* **2008,** *9* (6), 1579-1585.
17. Sehaqui, H.; Liu, A.; Zhou, Q.; Berglund, L. A., Fast Preparation Procedure for Large, Flat Cellulose and Cellulose/Inorganic Nanopaper Structures. *Biomacromolecules* **2010,** *11* (9), 2195-8.
18. Datsyuk, V.; Trotsenko, S.; Reich, S., Carbon-Nanotube–Polymer Nanofibers with High Thermal Conductivity. *Carbon* **2013,** *52*, 605-608.